

Unified-modal Salient Object Detection via Adaptive Prompt Learning

Kunpeng Wang

Chenglong Li

Zhengzheng Tu*

Bin Luo

Anhui University, China

kp.wang@foxmail.com, lc11314@foxmail.com, zhengzhengahu@163.com, luobin@ahu.edu.cn

Abstract

Existing single-modal and multi-modal salient object detection (SOD) methods focus on designing specific architectures tailored for their respective tasks. However, developing completely different models for different tasks leads to labor and time consumption, as well as high computational and practical deployment costs. In this paper, we make the first attempt to address both single-modal and multi-modal SOD in a unified framework called UniSOD. Nevertheless, assigning appropriate strategies to modality variable inputs is challenging. To this end, UniSOD learns modality-aware prompts with task-specific hints through adaptive prompt learning, which are plugged into the proposed pre-trained baseline SOD model to handle corresponding tasks, while only requiring few learnable parameters compared to training the entire model. Each modality-aware prompt is generated from a switchable prompt generation block, which performs structural switching solely relied on single-modal and multi-modal inputs. UniSOD achieves consistent performance improvement on 14 benchmark datasets for RGB, RGB-D, and RGB-T SOD, which demonstrates that our method effectively and efficiently unifies single-modal and multi-modal SOD tasks.

1. Introduction

Salient object detection (SOD) aims to identify and segment object(s) that attract human attention in an visible image. It can help eliminate redundant information and has been applied in many computer vision tasks, such as instance segmentation [35], object tracking [89], and video analysis [6, 12]. Though achieving great success [47, 65, 96], single-modal SOD still fails in some challenging scenes, e.g., low illumination, complex background, and similar foreground and background. To tackle these challenges, multi-modal SOD exploits the complementary benefits of RGB-Depth (RGB-D) [15, 23, 40, 88, 91] or RGB-Thermal (RGB-T) [44, 67–69] image pairs for robust prediction.

However, in real-world applications, depth and thermal

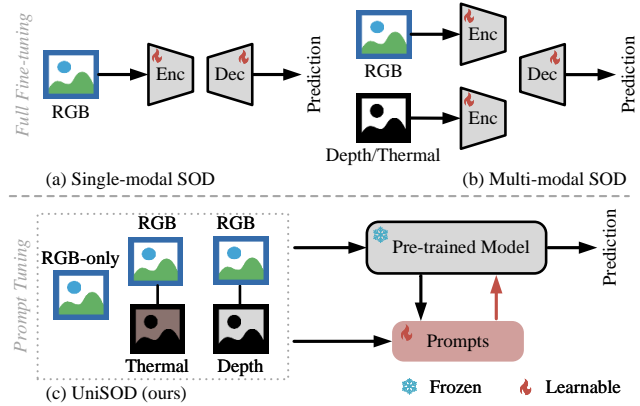


Figure 1. Workflow comparisons between existing Salient object detection (SOD) models with full fine-tuning and ours UniSOD with prompt tuning. (a) & (b) Existing single-modal and multi-modal SOD methods fully fine-tune the entire encoder-decoder based model, which is designed with a specific architecture tailored for the corresponding SOD task. (c) Compared to (a) & (b), the proposed UniSOD simultaneously handles single-modal and multi-modal inputs and only learns a few parameters of different task-specific prompts, which are simply plugged into a frozen pre-trained model to adapt to corresponding SOD tasks.

infrared sensors are not widely available [1, 18, 52, 94], and the corresponding multi-modal data are limited. In this case, the modality absence leads to poor performance of multi-modal models, even inferior to that of the single-modal ones [17, 27, 29]. To preserve performance, a straightforward notion is to train an extra single-modal SOD model from scratch only for visible images. In this way, different models need to be designed and trained separately for single-modal and multi-modal inputs. For example, Liu et al. [41] design a framework for both RGB and RGB-D SOD based on vision transformer. Different from the RGB SOD model, they use an exclusive cross modality transformer for the RGB-D SOD model to perform multi-modal information interaction. Zhou et al. [96] form an unsupervised framework for multiple SOD tasks through boundary-aware matching and saliency distilling.

Although effective, to adapt to both single-modal and multi-modal inputs, these methods design different specific models before training, which is laborious and increases the computational and deployment burden, especially for modern transformer-based methods [8, 44, 102] with more parameters.

Recently, prompt learning has attracted great attention as it boosts the performance of many Natural Language Processing (NLP) downstream tasks [30, 42] by only fine-tuning prompts. Some computer vision research [24, 29, 101] also show the great potential of prompt learning to be an alternative to full fine-tuning, which requires tuning a large number of parameters by training a model from scratch. The key of prompt learning is to learn task-specific cues for downstream inputs to exploit the general representation capabilities of the frozen pre-trained model. Inherently, single-modal and multi-modal SOD have different inputs but the same objective, implying the substantial overlap in prior knowledge regarding feature extraction and fusion. Therefore, it is natural to introduce prompt learning into SOD to efficiently utilize the prior knowledge of the pre-trained model and reduce the computational burden.

To this end, we propose a unified SOD framework, called UniSOD, for both single-modal and multi-modal SOD through prompt learning. For different input cases (i.e., RGB-only, RGB-D, RGB-T), we learn different prompts to drive the pre-trained model to address the corresponding tasks. Specifically, we proposed a simple but effective baseline SOD model for pre-training, which learns sufficient prior knowledge for saliency detection. Furthermore, a switchable prompt generation (SPG) block is proposed to perform structure switching based on single-modal and multi-modal inputs to generate modality-aware prompts. By combining each prompt with intermediate input features of the frozen pre-trained model for multi-stage interaction, UniSOD learns few additional prompt parameters to adapt the fine-tuning demands of different SOD tasks, including RGB, RGB-D, and RGB-T SOD. The main contributions of our work are summarized as follows:

- We are the first to propose a novel unified framework for RGB, RGB-D, and RGB-T SOD through prompt learning, which adapts the pre-trained model to both single-modal and multi-modal SOD tasks with few learnable parameters.
- The novel network consists of a simple and effective baseline SOD model for pre-training, which provides rich prior knowledge for downstream tasks, and a switchable prompt generation block that performs structure switching based on single-modal and multi-modal inputs to generate task-specific prompts.
- Extensive experiments on 14 benchmark datasets demonstrate the superior performance of our proposed UniSOD, with maximum improvement of 22.2%, 29.4%, and

19.0% on *MAE* metric for RGB, RGB-D, and RGB-T SOD, respectively, proving the effectiveness and potential of the proposed unified framework.

2. Related Work

2.1. Salient Object Detection

General salient object detection (SOD) aims to recognize and segment the most attractive objects from visible images. With the development of deep neural networks [16, 20, 60], numerous studies [74] have been presented based on boundary enhancement [59, 73, 87, 92], feature refinement [38, 80, 81, 93], multi-decoder [77, 78], attention mechanism [39, 76, 100], and uncertainty perception [31, 65, 75]. Recently, some methods [41, 47, 82] with impressive performance have been developed due to the long-range dependency modeling capabilities of Transformer [71]. However, these methods still struggle to tackle some challenging scenes, such as complex and low-contrast backgrounds, illumination changes, blur, etc. To deal with these inherent challenges, some studies introduce depth [15, 21, 22, 55, 58, 62, 88] or thermal [44, 63, 67, 69, 70, 99] images as complementary information for visible images. For example, Piao et al. [58] integrate multi-scale complementary cues from RGB and depth streams for accurate salient object location in complex background scenes. Sun et al. [62] utilize geometric priors in the depth map to enhance RGB features and reduce background interference, thus accurately capturing salient objects in complex scenes. To preserve performance in challenging scenes, Tu et al. [69] fuse features of RGB and thermal modalities through a multi-interactive dual decoder.

Nonetheless, the limited availability of depth and thermal sensors in practice leads to degraded performance of these multi-modal models, which is even inferior to that of single-modal ones [17, 27, 29]. Therefore, some recent studies [41, 96] tend to design methods that address both single-modal and multi-modal SOD, but require different structures and training. In addition, some methods [2, 90, 94] attempt to estimate depth information from visible images as a complement to the missing modality. However, the performance of these methods depends on the estimation module, which cannot guarantee the quality of the estimated features. In this paper, from a novel perspective, we utilize the capability of a pre-trained model through prompt tuning to address single-modal and multi-modal SOD uniformly, with a few parameters and low computational cost.

2.2. Prompt Learning in Computer Vision

In computer vision, full fine-tuning is widely employed to leverage the generalized representational capabilities of pre-trained models for downstream tasks. The common practice

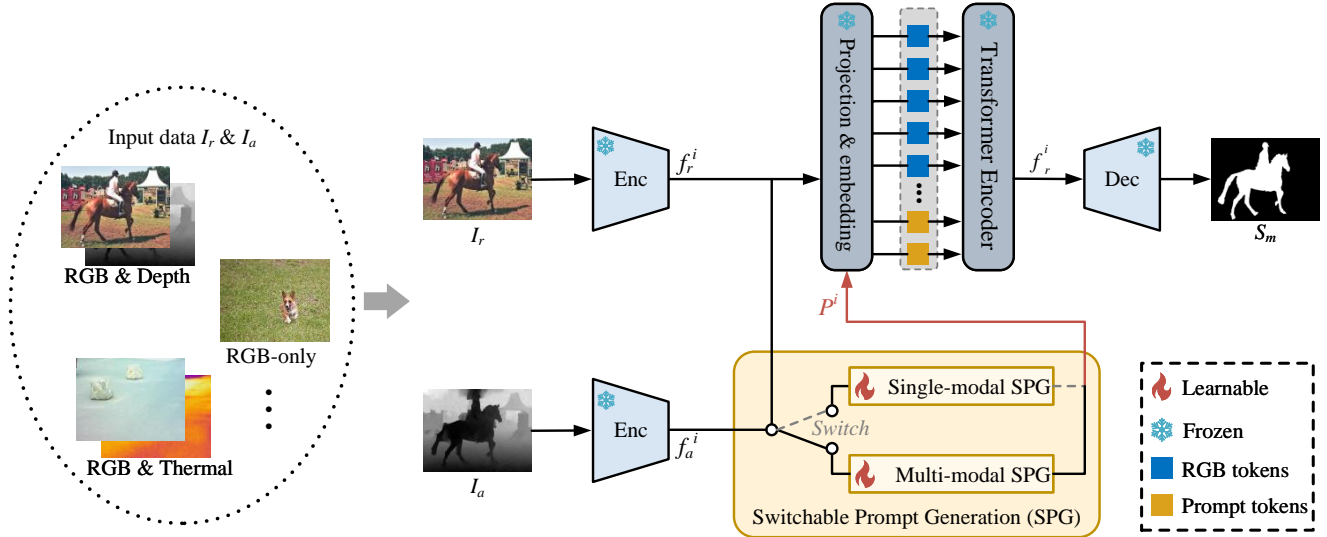


Figure 2. Overall architecture of our proposed UniSOD model for both single-modal and multi-modal SOD. The framework is based on the proposed baseline SOD model (see Fig. 3) whose parameters are all pre-trained and frozen here. The single-modal or multi-modal inputs are first fed to the same encoder to extract multi-level features. Then a switchable prompt generation (SPG) block is designed to generate task-specific prompts through structural switching based on single and multi-modal input features. By attaching the prompts to the intermediate RGB input features of the pre-trained model and feeding them into the transformer encoder, the prompts can be learned and drive the pre-trained model to address corresponding SOD tasks.

is to first train a common pre-trained model on a large-scale dataset, and then fine-tune the parameters of the entire pre-trained model in different downstream tasks. This approach results in satisfactory performance, but requires separate training and storage of all model parameters for different downstream tasks.

Recently, prompt learning demonstrates its efficiency in the field of nature language processing, which appends a prompt to the input to instruct the pre-trained model for downstream tasks. Consequently, visual prompts are also introduced into many computer vision tasks [9, 24, 29, 66, 101] to adapt the pre-trained model to downstream vision tasks by tuning few learnable parameters. For example, VPT [24] introduces additional few learnable parameters in the input space of the frozen pre-trained transformer model to adapt to downstream vision tasks. LPT [9] categorizes prompts into shared and specific ones to make the pre-trained model discriminative for long-tail data. ViPT [101] introduces prompts for a pre-trained single-modal tracker to adapt it to different multi-modal tracking tasks. However, it only designs prompts for multi-modal inputs, resulting in the pre-trained model that can only adapt to multi-modal tasks and can not adapt to single-modal tasks at the same time, which is not conducive to real-world applications. In addition, it generates prompts by summing the features of two modalities, which fails to perform sufficient multi-modal interactions and leads to poor exploitation of the pre-trained model. In this paper, we design a switchable

prompt generation block to interact single-modal or multi-modal inputs, which can adapt the pre-trained model to both single-modal and multi-modal SOD tasks.

3. Methodology

In this paper, we propose UniSOD to address both single-modal and multi-modal SOD in a unified way. Instead of designing multiple specific models for different tasks and fully fine-tuning the entire model, UniSOD only learns task-specific prompts with few learnable parameters to drive the pre-trained model to address the corresponding tasks.

3.1. Overview

Problem Definition. Given an visible image I_r of size $\mathbb{R}^{H \times W}$, the objective of single-modal SOD is to predict a saliency map S_m , where each scalar value $S_m^{i,j}$ represents the confidence of a pixel belonging to the foreground region. For multi-modal SOD, it introduces an additional modality for the original RGB modality, extends the input to $\{I_r, I_a\}$, where I_a represents depth or thermal image. The goal of multi-modal SOD is the same as that of single-modal SOD. Therefore, the key to unified SOD research is to make full use of their overlapping prior knowledge to efficiently address different SOD tasks.

Overall Framework. Fig. 2 shows an overall architecture of the proposed UniSOD model. Given a pre-trained SOD model, which has strong representation and discrimination capabilities for various features, we keep all its pa-

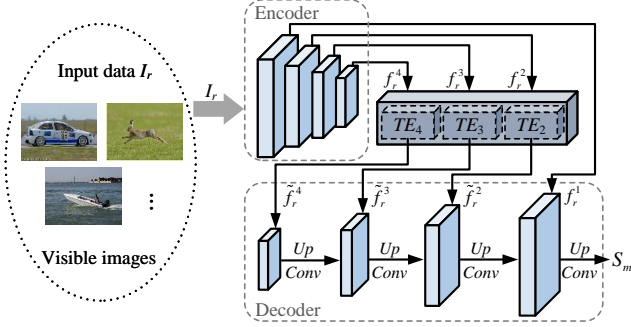


Figure 3. Detailed architecture of the pre-trained RGB SOD model.

rameters frozen to fully exploit the capabilities without impairing it. Considering the generalization ability of the pre-trained model, for input of any modality (i.e., I_r and I_a), we all send it to the same encoder to extract multi-level features. After that, each level of features is fed into a switchable prompt generation block (SPG) to produce task-specific prompts, which are then appended to the inherent input features. Therefore, the input space of the pre-trained transformer encoder is modified, and the parameters of the prompts are learned through the multi-layer transformer encoder and progressive decoder. In this way, for both single-modal and multi-modal inputs, the pre-trained model is driven by task-specific prompts to predict the corresponding saliency map.

3.2. Baseline SOD Model for Pre-training

The multi-modal SOD model can be viewed as an extension of the single-modal SOD (i.e., RGB SOD) model by adding a stream for the extra modality (i.e., depth or thermal modality) based on the original RGB stream, and the two streams use the same backbone in most methods [44, 55, 97]. In addition, both single-modal and multi-modal SOD have the same purpose of predicting the foreground region in the image(s) so as to obtain the final saliency map. Therefore, we attempt to use a pre-trained model with an RGB SOD framework to maximize the inclusion of prior knowledge common to both single-modal and multi-modal SOD. However, existing RGB SOD frameworks [54, 59, 76] are almost designed for specific problems, which impairs the generalization ability of the pre-trained model to various kinds of data. Moreover, their framework structure is complex and is difficult to be extended to different downstream tasks. To this end, we design a simple and effective baseline SOD framework for pre-training, as shown in Fig. 3.

Model Architecture. The framework contains three components: an encoder for feature extraction, a transformer encoder for integrating the extracted features, and a decoder for feature reconstruction. Considering the strong

feature representation ability of Swin Transformer [43], we adopt it with pre-trained weights as the backbone in the encoder, the same as [44]. In this way, the input image I_r is first split into non-overlapping patches, and neighboring patches are merged as the backbone deepens. Then, hierarchical feature representations are constructed, denoted as $\{f_r^i\}_{i=1}^4$. To further integrate the extracted features, we flatten and feed them into a L -layer standard vision transformer encoder, which has the ability to model long-range dependencies. This process is formulated as:

$$\tilde{f}_r^i = \text{reshape}(TE_i(\text{flatten}(f_r^i))), i = 2, \dots, 4, \quad (1)$$

where f_r^i is the output feature after reshaping. TE_i denotes the i th level transformer encoder, which contains multi-head self-attention, layer norm, feed-forward network, and residual connection, and we refer readers to the literature [10] for more detailed descriptions. Note that the extracted features of the first level are not fed into the transformer encoder due to the heavy computational burden of large resolution data. Subsequently, the decoder aggregates multi-level features in a top-down manner to progressively reconstruct high-resolution feature maps for final prediction, which can be formulated as:

$$f_s^i = \begin{cases} \text{Conv}_{3 \times 3}(\text{Up}_2(\tilde{f}_r^i)), & i = 4, \\ \text{Conv}_{3 \times 3}(\text{Up}_2(\tilde{f}_r^i + f_s^{i+1})), & i = 2, 3, \end{cases} \quad (2)$$

$$S_m = \text{Conv}_{3 \times 3}(\text{Up}_4(\text{Conv}_{3 \times 3}(f_s^2 + f_r^1))), \quad (3)$$

where S_m represents the predicted saliency map, $\text{Conv}_{3 \times 3}$ is a 3×3 convolutional layer, Up_x is the $x \times$ upsampling operation with bilinear interpolation. We introduce the first-level features here to supplement detailed information.

Optimization Objective. For the pre-trained model, we fine-tune all its parameters during the training process. Following [69, 79], we use a combination of binary cross-entropy loss, smoothness loss [19], and dice loss [50] as the overall loss function to optimize our method,

$$\mathcal{L} = \mathcal{L}_{bce} + \mathcal{L}_{smooth} + \mathcal{L}_{dice}, \quad (4)$$

where \mathcal{L}_{bce} , \mathcal{L}_{smooth} , and \mathcal{L}_{dice} denote the binary cross-entropy loss, smoothness loss, and dice loss, respectively, between the predicted saliency map S_m and ground truth.

3.3. Switchable Prompt Generation

Existing SOD methods almost exclusively design frameworks for single-modal or multi-modal SOD tasks, or design different frameworks for both. However, designing and training different models for different tasks is laborious and resource-intensive. Therefore, a model that uniformly and efficiently addresses both single-modal and multi-modal

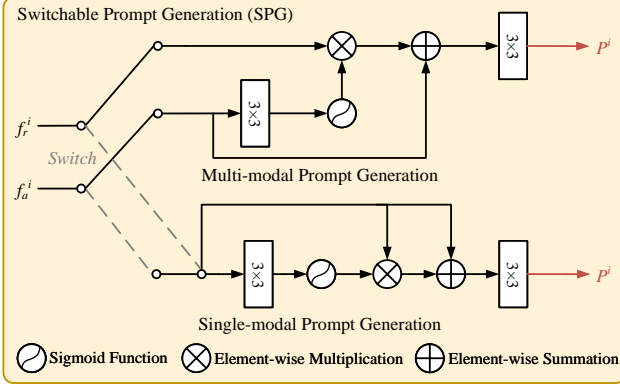


Figure 4. Detailed design of the proposed SPG block. The SPG adaptively switches the structure based on single-modal and multi-modal inputs to generate task-specific prompts.

SOD is needed to cope with different situations in real-world applications. Some recent works [9, 24, 101] introduce a small number of parameters to the frozen pre-trained model to learn visual prompts. By fine-tuning them during training, they achieve impressive results on many downstream tasks. In particular, ViPT [101] generates prompts by exploiting inter-modal information to adapt a pre-trained single-modal tracker to address different multi-modal tracking tasks. However, it only learns prompts for multi-modal inputs, leading to the failure to address single-modal tasks at the same time. Although this issue can be addressed by adjusting the network structure and reusing the ability of the pre-trained single-modal model, this is inefficient and similar to training different models for different tasks.

To address the above issue, we propose a switchable prompt generation (SPG) block that performs a structural switching solely relied on single-modal and multi-modal inputs to generate task-specific prompts, which drive the frozen pre-trained RGB SOD model to address corresponding SOD tasks with few learnable parameters. Considering that the feature representations of different levels jointly contribute to the recognition of salient regions, we build a SPG block for each level of the extracted features to fully adapt the pre-trained model to different tasks.

Multi-modal Prompt. In this case, the goal of the SPG block is to exploit the complementary benefits of two modalities to generate robust prompts. By combining them with the inherent RGB intermediate features as input to the subsequent components, the multi-modal information can be integrated to deal with complex scenes and the pre-trained model can be instructed to address the corresponding multi-modal SOD task. The upper part of Fig. 4 illustrates the structure of the SPG for multi-modal inputs. Specifically, given the extracted features $\{f_r^i, f_a^i\}_{i=1}^4$ of two modalities in the i -th level, we first utilize a 3×3 convolu-

tional layer to integrate the auxiliary-modal feature, which learns the properties of the unfamiliar modality (i.e., depth or thermal modality). Then, a sigmoid function is employed to squeeze the feature values to the $[0,1]$ range as a mask μ , which guides the RGB feature to focus on the common information between modalities through element-wise multiplication. To further complement the information of the auxiliary modality, the original extracted auxiliary-modal feature is added to the guided RGB feature with a residual connection. Subsequently, the prompt is obtained by performing a 3×3 convolution on the multi-modal feature. The whole process can be formulated as:

$$\mu = \sigma (Conv_{3 \times 3} (f_a^i)), \quad (5)$$

$$P^i = Conv_{3 \times 3} (f_r^i \odot \mu + f_a^i), \quad (6)$$

where P^i denotes the prompt of the i -th level, \odot is the element-wise multiplication, and σ is the sigmoid function.

Single-modal Prompt. In this case, with no novel inputs, the goal of the SPG block becomes to refine the inherent RGB features to generate single-modal prompts, which facilitate saliency cue mining in subsequent modules and thus drive the pre-trained model to address the RGB SOD task. In specific, since the parameters of the backbone are frozen, as the two inputs to the model become the same visible image, the two extracted features $\{f_r^i, f_r^i\}_{i=1}^4$ at each level are also the same. In this way, the structure of the SPG is switched as shown in the lower part of Fig. 4. The 3×3 convolutional layer here is used on the RGB feature to further expand the receptive field and extract more useful information, which is compressed into a mask μ by the sigmoid function. Then, the original RGB feature f_r^i is guided by it through element-wise multiplication, followed by a residual connection to obtain the refined feature. The single-modal prompt P^i is obtained by integrating the refined RGB feature with a 3×3 convolution, which can be formulated as:

$$\mu = \sigma (Conv_{3 \times 3} (f_r^i)), \quad (7)$$

$$P^i = Conv_{3 \times 3} (f_r^i \odot \mu + f_r^i), \quad (8)$$

Optimization To optimize the prompts, we sum them with the original RGB features and send them into the multi-layer transformer encoder, the same as in [24]. The loss function \mathcal{L} used is the same as that of the pre-trained model. During training, the data flow propagates through the entire model that contains the frozen pre-trained model and the learnable prompts, which only account for 18% of the entire model parameters but drive the pre-trained model to achieve superior performance on both single-modal and multi-modal SOD tasks.

Table 1. Quantitative comparison of our proposed UniSOD with other 16 RGB SOD methods on 5 representative datasets. The best and second-best results are marked with red and blue, respectively. The symbols ‘↑’ / ‘↓’ indicate that a higher / lower score is better.

Method	AFNet ₁₉ [14]	CPD ₁₉ [81]	BASNet ₁₉ [59]	PoolNet ₁₉ [37]	MINet ₂₀ [54]	LDF ₂₀ [78]	GateNet ₂₀ [93]	F3Net ₂₀ [77]	PAKRN ₂₁ [83]	PFSNet ₂₁ [46]	VST ₂₁ [41]	EDN ₂₂ [80]	ICON ₂₃ [102]	MENet ₂₃ [76]	BBRF ₂₃ [47]	SelfReformer ₂₃ [86]	UniSOD (Ours)	
Params (M)	↓	36.0	47.9	87.1	68.3	162.4	25.2	128.6	25.5	45.2	31.2	32.2	42.8	92.4	-	74.1	44.6	25.1
DUTS	E_{ϵ} ↑	0.879	0.886	0.884	0.881	0.898	0.910	0.891	0.902	0.916	0.902	0.892	0.908	0.930	0.921	0.927	0.921	0.937
	S_m ↑	0.867	0.869	0.866	0.879	0.884	0.892	0.890	0.888	0.900	0.892	0.896	0.892	0.917	0.905	0.909	0.911	0.924
	F_{β}^w ↑	0.785	0.795	0.803	0.796	0.825	0.845	0.818	0.835	0.861	0.842	0.828	0.845	0.886	0.870	0.886	0.872	0.905
	MAE ↓	0.046	0.043	0.048	0.042	0.037	0.037	0.034	0.038	0.035	0.033	0.036	0.037	0.035	0.025	0.028	0.025	0.027
ECSSD	E_{ϵ} ↑	0.918	0.925	0.921	0.921	0.927	0.925	0.924	0.927	0.924	0.928	0.918	0.929	0.932	0.925	0.934	0.929	0.940
	S_m ↑	0.913	0.918	0.916	0.917	0.925	0.924	0.920	0.924	0.928	0.930	0.932	0.927	0.941	0.928	0.939	0.936	0.949
	F_{β}^w ↑	0.886	0.898	0.904	0.890	0.911	0.915	0.894	0.912	0.918	0.920	0.910	0.918	0.936	0.920	0.944	0.926	0.952
	MAE ↓	0.042	0.037	0.037	0.042	0.033	0.034	0.040	0.033	0.032	0.031	0.033	0.032	0.023	0.031	0.022	0.027	0.018
OMRON	E_{ϵ} ↑	0.853	0.866	0.869	0.857	0.865	0.874	0.862	0.870	0.885	0.875	0.861	0.879	0.898	0.882	0.891	0.889	0.904
	S_m ↑	0.826	0.825	0.836	0.832	0.833	0.839	0.838	0.838	0.853	0.842	0.850	0.849	0.869	0.850	0.861	0.861	0.871
	F_{β}^w ↑	0.717	0.719	0.751	0.721	0.738	0.752	0.729	0.747	0.779	0.756	0.755	0.770	0.804	0.771	0.803	0.784	0.813
	MAE ↓	0.057	0.056	0.056	0.056	0.056	0.052	0.055	0.053	0.050	0.055	0.050	0.049	0.043	0.045	0.044	0.043	0.041
HKU-IS	E_{ϵ} ↑	0.942	0.944	0.946	0.950	0.953	0.954	0.949	0.953	0.955	0.956	0.953	0.956	0.965	0.960	0.965	0.959	0.968
	S_m ↑	0.905	0.905	0.909	0.916	0.919	0.919	0.915	0.917	0.924	0.924	0.928	0.924	0.935	0.927	0.932	0.931	0.940
	F_{β}^w ↑	0.869	0.875	0.889	0.883	0.897	0.904	0.880	0.900	0.909	0.910	0.897	0.908	0.925	0.917	0.932	0.915	0.938
	MAE ↓	0.036	0.034	0.032	0.032	0.029	0.028	0.033	0.028	0.027	0.026	0.029	0.026	0.022	0.023	0.020	0.024	0.018
PASCAL-S	E_{ϵ} ↑	0.851	0.855	0.852	0.845	0.857	0.871	0.857	0.865	0.863	0.862	0.843	0.870	0.875	0.870	0.873	0.879	0.886
	S_m ↑	0.849	0.848	0.838	0.851	0.856	0.862	0.857	0.860	0.858	0.860	0.871	0.864	0.885	0.871	0.878	0.881	0.889
	F_{β}^w ↑	0.798	0.800	0.798	0.791	0.815	0.828	0.803	0.822	0.823	0.825	0.822	0.833	0.860	0.844	0.862	0.854	0.876
	MAE ↓	0.070	0.070	0.075	0.071	0.063	0.059	0.068	0.062	0.066	0.063	0.061	0.061	0.048	0.054	0.049	0.051	0.043

Table 2. Quantitative comparison of our proposed UniSOD with other 16 RGB-D SOD methods on 6 representative datasets.

Method	HAINet ₂₁ [34]	SPNet ₂₁ [97]	RD3D ₂₁ [3]	DSA2F ₂₁ [62]	DCF ₂₁ [21]	VST ₂₁ [41]	MobileSal ₂₂ [79]	SSL ₂₂ [95]	MoAD ₂₂ [25]	CIRNet ₂₂ [7]	DIGRN ₂₃ [5]	HRTans ₂₃ [63]	LSNet ₂₃ [99]	CAVER ₂₃ [55]	CATNet ₂₃ [61]	PICRN ₂₃ [8]	UniSOD (Ours)	
Params (M)	↓	59.8	150.3	28.9	34.0	97.0	53.5	6.5	74.2	5.0	103.2	166.7	26.3	4.6	55.8	263.1	86.0	25.1
DUT-RGBD	E_{ϵ} ↑	0.937	0.876	0.949	0.950	0.952	0.960	0.936	0.927	0.949	0.951	0.948	0.972	0.927	0.955	0.971	0.967	0.974
	S_m ↑	0.909	0.803	0.932	0.921	0.924	0.943	0.896	0.889	0.927	0.932	0.926	0.951	0.886	0.931	0.953	0.943	0.952
	F_{β}^w ↑	0.887	0.747	0.913	0.914	0.913	0.926	0.869	0.859	0.911	0.908	0.902	0.949	0.856	0.920	0.945	0.935	0.952
	MAE ↓	0.038	0.085	0.031	0.030	0.030	0.025	0.044	0.046	0.031	0.031	0.033	0.018	0.049	0.029	0.020	0.022	0.017
NJUD	E_{ϵ} ↑	0.917	0.931	0.918	0.923	0.922	0.913	0.914	0.881	0.909	0.922	0.928	0.929	0.891	0.922	0.932	0.930	0.940
	S_m ↑	0.909	0.925	0.915	0.903	0.903	0.922	0.905	0.841	0.906	0.915	0.932	0.926	0.837	0.920	0.932	0.924	0.932
	F_{β}^w ↑	0.882	0.909	0.890	0.889	0.884	0.892	0.874	0.786	0.881	0.881	0.909	0.914	0.775	0.903	0.921	0.909	0.925
	MAE ↓	0.039	0.029	0.037	0.039	0.038	0.035	0.040	0.065	0.041	0.040	0.028	0.029	0.074	0.032	0.026	0.030	0.025
NLPR	E_{ϵ} ↑	0.951	0.957	0.957	0.950	0.956	0.953	0.950	0.954	0.945	0.955	0.955	0.968	0.955	0.959	0.967	0.965	0.967
	S_m ↑	0.921	0.928	0.929	0.918	0.921	0.931	0.920	0.919	0.915	0.933	0.935	0.942	0.918	0.929	0.940	0.935	0.937
	F_{β}^w ↑	0.884	0.899	0.894	0.889	0.892	0.891	0.878	0.885	0.875	0.889	0.895	0.921	0.881	0.899	0.916	0.911	0.919
	MAE ↓	0.025	0.021	0.022	0.024	0.023	0.024	0.025	0.025	0.027	0.027	0.023	0.023	0.016	0.024	0.022	0.018	0.019
SIP	E_{ϵ} ↑	0.924	0.930	0.919	0.908	0.920	0.936	0.914	0.921	0.908	0.917	0.918	0.943	0.911	0.927	0.943	0.916	0.941
	S_m ↑	0.886	0.894	0.885	0.861	0.873	0.903	0.873	0.880	0.865	0.888	0.885	0.909	0.909	0.893	0.911	0.865	0.899
	F_{β}^w ↑	0.860	0.873	0.852	0.838	0.850	0.878	0.837	0.851	0.828	0.848	0.849	0.901	0.877	0.874	0.897	0.838	0.896
	MAE ↓	0.049	0.043	0.049	0.057	0.051	0.040	0.054	0.049	0.058	0.053	0.053	0.035	0.040	0.043	0.035	0.056	0.036
SSD	E_{ϵ} ↑	0.843	0.910	0.905	0.904	0.898	0.907	0.898	0.833	0.894	0.898	0.889	0.910	0.902	0.915	0.621	0.915	0.930
	S_m ↑	0.769	0.871	0.863	0.876	0.852	0.889	0.863	0.745	0.854	0.862	0.866	0.867	0.856	0.874	0.417	0.878	0.882
	F_{β}^w ↑	0.682	0.831	0.794	0.836	0.800	0.836	0.804	0.638	0.801	0.791	0.804	0.820	0.796	0.826	0.114	0.837	0.857
	MAE ↓	0.101	0.044	0.052	0.047	0.053	0.045	0.052	0.100	0.057	0.054	0.053	0.045	0.055	0.044	0.232	0.046	0.034
STERE	E_{ϵ} ↑	0.930	0.930	0.926	0.928	0.931	0.916	0.916	0.923	0.914	0.921	0.927	0.929	0.913	0.931	0.935	0.937	0.938
	S_m ↑	0.909	0.907	0.911	0.897	0.905	0.913	0.903	0.897	0.898	0.891	0.916	0.921	0.871	0.914	0.921	0.920	0.924
	F_{β}^w ↑	0.877	0.879	0.877	0.877	0.880	0.872	0.865	0.864	0.861	0.836	0.877	0.899	0.827	0.887	0.900	0.898	0.909
	MAE ↓	0.038	0.037	0.038	0.038	0.037	0.038	0.041	0.042	0.042	0.049	0.038	0.030	0.054	0.034	0.030	0.031	0.027

4. Experiments

4.1. Experimental Settings

UniSOD achieves the unification of single-modal and multi-modal SOD tasks. In this paper, we verify the effectiveness and generalization of the proposed method on three main tasks. We perform prompt-tuning for these downstream tasks without specific modulation and all experimental settings are kept consistent. Due to space limitations, more experimental results are provided in **supp**.

Datasets. (i) For RGB SOD, we evaluate different methods on six prevalent benchmark datasets, including DUTS [72] (10,553 training images and 5,019 testing images), OMRON [85] (5,168 images), ECSSD [84] (1,000 images), HKU-IS [32] (4,447 images), PASCAL-S [36] (850 images), and SOD [51] (300 images). (ii) For RGB-D

SOD, all methods are assessed on six popular benchmark datasets, including DUT-RGBD [23] (1,200 image pairs), NJUD [26] (1,985 image pairs), NLPR [56] (1,000 image pairs), SSD [33] (80 image pairs), SIP [13] (929 image pairs), and STERE [53] (1,000 image pairs). (iii) For RGB-T SOD, we provide the experimental results of all methods on three prevalent benchmark datasets: VT5000 [67] (2,500 training image pairs and 2,500 testing image pairs) (821 image pairs), VT1000 [68] (1,000 image pairs), and VT821 [64]. During the training process, following [62, 70, 96], we use the training set of DUTS [72] for RGB SOD models, a collection of 2985 samples from NLPR [56], NJUD [26], and DUT-RGBD [23] for RGB-D models, and the training set of VT5000 [67] for RGB-T models.

Evaluation Metrics. We employ four widely used evaluation metrics to assess the performance of different

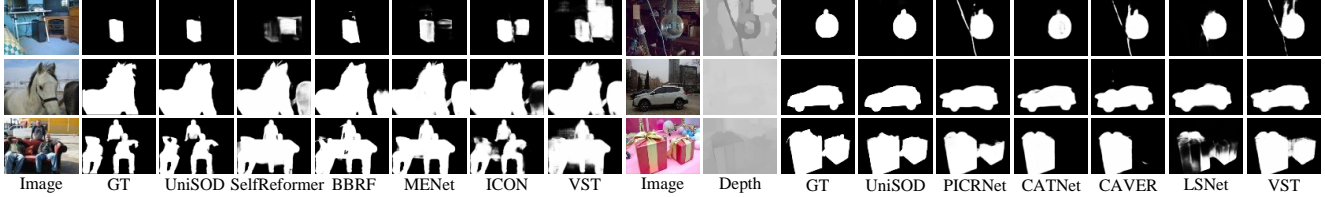


Figure 5. Qualitative comparisons of our proposed UniSOD with recent state-of-the-art RGB (left) and RGB-D (right) SOD methods in some challenging scenes. (GT: ground truth)

Table 3. Quantitative comparison of our proposed UniSOD with other 6 recent RGB-T SOD methods on 3 representative datasets.

Method	SwinNet ₂₂ [44]	MCFNet ₂₃ [48]	HRTrans ₂₃ [63]	LSNet ₂₃ [99]	CAVER ₂₃ [55]	WaveNet ₂₃ [98]	UniSOD (Ours)
Params (M) ↓	199.2	70.8	26.3	4.6	55.8	80.7	25.1
VT5000							
E_ξ ↑	0.942	0.924	0.945	0.915	0.924	0.940	0.953
S_m ↑	0.912	0.887	0.912	0.877	0.892	0.911	0.919
F_β^w ↑	0.846	0.836	0.870	0.806	0.835	0.864	0.889
MAE ↓	0.026	0.033	0.025	0.037	0.032	0.026	0.021
VT1000							
E_ξ ↑	0.947	0.944	0.945	0.935	0.945	0.952	0.956
S_m ↑	0.938	0.932	0.938	0.925	0.936	0.945	0.945
F_β^w ↑	0.894	0.906	0.913	0.887	0.909	0.921	0.929
MAE ↓	0.018	0.019	0.017	0.023	0.017	0.015	0.014
VT821							
E_ξ ↑	0.926	0.918	0.929	0.911	0.919	0.929	0.932
S_m ↑	0.904	0.891	0.906	0.878	0.891	0.912	0.911
F_β^w ↑	0.818	0.835	0.849	0.809	0.835	0.863	0.868
MAE ↓	0.030	0.029	0.026	0.033	0.033	0.024	0.026

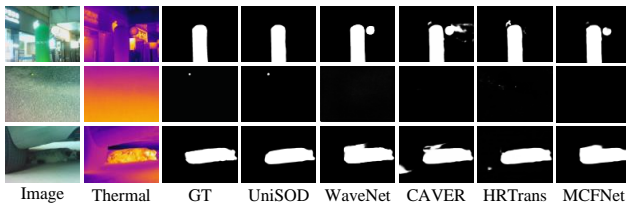


Figure 6. Qualitative comparisons of our proposed UniSOD with recent state-of-the-art RGB-T SOD methods in some challenging scenes.

methods comprehensively. In specific, E-measure [11] (E_ξ) measures both image-level and pixel-level errors. S-measure [4] (S_m) evaluates the structural similarity at the region and object level. Weighted F-measure [49] (F_β^w) uses weighted precision and recall to measure region-based similarity. Mean Absolute Error [57] (MAE) indicates the absolute error between the prediction and ground truth. To assess model complexity, we also report the number of parameters (Params).

Implementation Details. The framework is implemented with PyTorch in a workspace with two RTX 3090 GPUs. All input images are resized into 384×384 for training and inferring. The backbone network is equipped with SwinB [43] whose parameters are trained on ImageNet [28]. The AdamW [45] algorithm with a learning rate of $1e-5$ is used to optimize both the pre-trained model and the fine-tuned models. For the pre-trained model, we set the batch size as 4 and train for a total of 200 epochs. For all the downstream models, the frozen parameters are initialized

with the pre-trained model, and the trainable parameters are random initialized. The batch size is set to 8 and a total of 300 epochs are trained for prompt learning.

4.2. Comparison with State-of-the-arts

For single-modal SOD, we compare the proposed UniSOD with 16 state-of-the-art RGB SOD methods, including AFNet [14], CPD [81], BASNet [59], PoolNet [37], MINet [54], LDF [78], GateNet [93], F3Net [77], KRN [83], PFSNet [46], VST [41], EDN [80], ICON [102], MENet [76], BBRF [47], and SelfReformer [86]. For multi-modal SOD, we compare the proposed UniSOD with 16 state-of-the-art RGB-D SOD methods, including HAINet [34], SPNet [97], RD3D [3], DSA2F [62], DCF [21], VST [41], MobileSal [79], SSL [95], MoAD [25], CIRNet [7], DIGRNet [5], HRTrans [63], LSNet [99], CAVER [55], CATNet [61], and PICRNet [8]. We also compare the proposed UniSOD with 6 recent state-of-the-art RGB-T SOD methods, including SwinNet [44], MCFNet [48], HRTrans [63], LSNet [99], CAVER [55], and WaveNet [98].

Table 1, Table 2, and Table 3 show the quantitative comparison results on RGB, RGB-D, and RGB-T datasets, respectively. It can be found that our UniSOD with comparable learnable parameters achieves superior performance on both single-modal and multi-modal SOD tasks, demonstrating the effectiveness of our method. This is mainly because the SPG block with few parameters effectively drive the pre-trained model through prompt learning. In addition, Figs. 5 and 6 illustrate the visual comparison between our UniSOD and the advanced methods. The results show that our method is able to deal with different challenging scenes, such as complex background, scale variation, and modality failure.

4.3. Ablation Study

In this section, we perform ablation studies to illustrate the effectiveness of the components in our method. The results on five single-modal (i.e., DUTS and ECSSD) and multi-modal (i.e., STERE, NJUD, and VT5000) datasets are shown in Table 4, in which the first line (i.e., UniSOD) shows the performance of our full model.

Table 4. Ablation studies of our proposed UniSOD on five single-modal and multi-modal datasets. 'w/o' means to remove the component. 'Prompt-cat' refers to inserting prompts in the input space through concatenation. 'UniSOD-X' denotes the pre-trained model driven with prompts specific to the X SOD task. The best results are marked with **bold**.

Model	Params (M)	DUTS				ECSSD				STERE				NJUD				VT5000			
		$E_\xi \uparrow$	$S_m \uparrow$	$F_\beta^\omega \uparrow$	$MAE \downarrow$	$E_\xi \uparrow$	$S_m \uparrow$	$F_\beta^\omega \uparrow$	$MAE \downarrow$	$E_\xi \uparrow$	$S_m \uparrow$	$F_\beta^\omega \uparrow$	$MAE \downarrow$	$E_\xi \uparrow$	$S_m \uparrow$	$F_\beta^\omega \uparrow$	$MAE \downarrow$	$E_\xi \uparrow$	$S_m \uparrow$	$F_\beta^\omega \uparrow$	$MAE \downarrow$
UniSOD	25.1	0.937	0.924	0.905	0.021	0.940	0.949	0.952	0.018	0.938	0.924	0.909	0.027	0.940	0.932	0.925	0.025	0.953	0.919	0.889	0.021
Pre-trained model	144.6	0.937	0.923	0.904	0.021	0.939	0.948	0.951	0.019	0.905	0.903	0.879	0.038	0.909	0.913	0.900	0.034	0.944	0.902	0.868	0.026
w/o SPG	144.6	0.925	0.907	0.879	0.026	0.928	0.934	0.933	0.024	0.877	0.857	0.817	0.059	0.889	0.885	0.861	0.045	0.934	0.887	0.840	0.029
Full fine-tuning	169.7	0.934	0.922	0.902	0.022	0.938	0.947	0.950	0.019	0.933	0.920	0.902	0.030	0.935	0.933	0.927	0.025	0.952	0.917	0.882	0.022
Prompt-concat	25.1	0.937	0.924	0.904	0.021	0.939	0.948	0.951	0.019	0.935	0.920	0.901	0.030	0.928	0.922	0.909	0.030	0.948	0.913	0.878	0.024

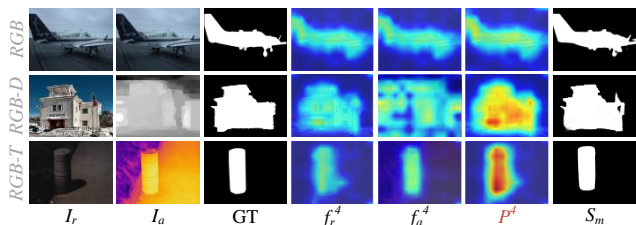


Figure 7. Feature visualization for the SPG block of the highest layer. I_r and I_a are input images, f_r^A and f_a^A are input features for SPG, P^A is the output prompt of SPG, and S_m is the prediction.

Effectiveness of the baseline SOD model. To verify the effectiveness of the proposed pre-trained baseline SOD model, we directly evaluate its performance on both single-modal and multi-modal datasets using only visible images as input, denoted as 'Pre-trained model' in Table 4. Compared with the advanced RGB SOD methods in Table 1, it can be found that our pre-trained model has superior performance with a simple structure and acceptable parameters, which indicates that it has great potential for exploration. Compared to the multi-modal methods in Tables 2 and 3, the advantages of our pre-trained model are not obvious, which confirms that a specific single-modal SOD model is difficult to handle multi-modal SOD tasks well at the same time. In addition, the comparison between the first and second rows of Table 4 shows that our full model can fully utilize the prior knowledge of the pre-trained model on both single-modal and multi-modal SOD tasks.

Effectiveness of SPG. We also remove the SPG block directly from the full model, which means that the RGB or auxiliary modality features of the other stream are directly summed into the intrinsic RGB stream as inputs to the following components. The results in the third row (i.e., w/o SPG) of Table 4 verify the positive effect of the SPG block. Compared with UniSOD, the performance drops by an average of 3.5%, 4.0%, 5.9%, and 49.9% in the four metrics (E_ξ , S_m , F_β^ω , and MAE) respectively. It is worth noting that its performance is also inferior to that of the pre-trained model that uses only visible image as input, especially on the multi-modal tasks. This is mainly because the additional input stream without prompt learning breaks the structure of the pre-trained model, leading to performance degradation.

Fig. 8 further vividly illustrates the visualization of the input features (f_r^A and f_a^A) and output features (P^A) of the SPG block. For single-modal input, the SPG block enhances the representation of input features through refinement, such as object boundaries and highlights, which prompts the pre-trained model to distinguish foreground regions more accurately, as shown in the first row of Fig. 8. For multi-modal inputs, the SPG block exploits the complementary benefits of the two modalities to drive the pre-trained model to deal with challenging scenes, such as depth ambiguity (second row), and low illumination (third row).

Effectiveness of prompt learning. In order to observe the effectiveness of prompt learning, we fine-tune the entire model that contains the pre-trained model and prompts, with results shown in the fourth row (i.e., 'Full fine-tuning') of Table 4. It can be found that with more training parameters its performance is comparable to that of our UniSOD on the single-modal SOD task, but inferior to our UniSOD on the multi-modal SOD tasks. This is mainly because plenty of parameters require more training data to learn them well, while the amount of multi-modal SOD data is limited. In addition, we perform the experiment to insert prompts into the input space through concatenation, denoted as 'Prompt-concat' in Table 4. The results show that the summation used by UniSOD has a better performance overall.

5. Conclusion

In this paper, we are the first to address both single-modal and multi-modal SOD tasks in a unified framework. To handle the difficulty of input modality variations, we propose the UniSOD to learn modality-aware prompts through adaptive prompt learning with few learnable parameters, which can drive pre-trained models to address the corresponding tasks. To this end, two components are proposed. The baseline SOD model provides rich prior knowledge for both single-modal and multi-modal downstream SOD tasks with a simple and effective structure. The SPG block is cleverly designed to perform the structural switching based on single-modal and multi-modal inputs. Experimental results on 14 benchmark datasets show that our UniSOD achieves superior performance for RGB, RGB-D, and RGB-T SOD, which demonstrates its great effectiveness and potential.

References

- [1] Vincent Casser, Sören Pirk, Reza Mahjourian, and Anelia Angelova. Depth prediction without the sensors: Leveraging structure for unsupervised learning from monocular videos. In *The Thirty-Third AAAI Conference on Artificial Intelligence, AAAI 2019, The Thirty-First Innovative Applications of Artificial Intelligence Conference, IAAI 2019, The Ninth AAAI Symposium on Educational Advances in Artificial Intelligence, EAAI 2019, Honolulu, Hawaii, USA, January 27 - February 1, 2019*, pages 8001–8008. AAAI Press, 2019. [1](#)
- [2] Chenglizhao Chen, Jipeng Wei, Chong Peng, Weizhong Zhang, and Hong Qin. Improved saliency detection in RGB-D images using two-phase depth estimation and selective deep fusion. *IEEE Trans. Image Process.*, 29:4296–4307, 2020. [2](#)
- [3] Qian Chen, Ze Liu, Yi Zhang, Keren Fu, Qijun Zhao, and Hongwei Du. RGB-D salient object detection via 3d convolutional neural networks. In *Thirty-Fifth AAAI Conference on Artificial Intelligence, AAAI 2021, Thirty-Third Conference on Innovative Applications of Artificial Intelligence, IAAI 2021, The Eleventh Symposium on Educational Advances in Artificial Intelligence, EAAI 2021, Virtual Event, February 2-9, 2021*, pages 1063–1071. AAAI Press, 2021. [6](#), [7](#)
- [4] Ming-Ming Cheng and Deng-Ping Fan. Structure-measure: A new way to evaluate foreground maps. *Int. J. Comput. Vis.*, 129(9):2622–2638, 2021. [7](#)
- [5] Xiaolong Cheng, Xuan Zheng, Jialun Pei, He Tang, Zehua Lyu, and Chuanbo Chen. Depth-induced gap-reducing network for RGB-D salient object detection: An interaction, guidance and refinement approach. *IEEE Trans. Multim.*, 25:4253–4266, 2023. [6](#), [7](#)
- [6] Runmin Cong, Jianjun Lei, Huazhu Fu, Fatih Porikli, Qingming Huang, and Chunping Hou. Video saliency detection via sparsity-based reconstruction and propagation. *IEEE Trans. Image Process.*, 28(10):4819–4831, 2019. [1](#)
- [7] Runmin Cong, Qinwei Lin, Chen Zhang, Chongyi Li, Xiaochun Cao, Qingming Huang, and Yao Zhao. Cir-net: Cross-modality interaction and refinement for RGB-D salient object detection. *IEEE Trans. Image Process.*, 31: 6800–6815, 2022. [6](#), [7](#)
- [8] Runmin Cong, Hongyu Liu, Chen Zhang, Wei Zhang, Feng Zheng, Ran Song, and Sam Kwong. Point-aware interaction and cnn-induced refinement network for RGB-D salient object detection. In *Proceedings of the 31st ACM International Conference on Multimedia, MM 2023, Ottawa, ON, Canada, 29 October 2023- 3 November 2023*, pages 406–416. ACM, 2023. [2](#), [6](#), [7](#)
- [9] Bowen Dong, Pan Zhou, Shuicheng Yan, and Wangmeng Zuo. LPT: long-tailed prompt tuning for image classification. In *The Eleventh International Conference on Learning Representations, ICLR 2023, Kigali, Rwanda, May 1-5, 2023*. OpenReview.net, 2023. [3](#), [5](#)
- [10] Alexey Dosovitskiy, Lucas Beyer, Alexander Kolesnikov, Dirk Weissenborn, Xiaohua Zhai, Thomas Unterthiner, Mostafa Dehghani, Matthias Minderer, Georg Heigold, Sylvain Gelly, Jakob Uszkoreit, and Neil Houlsby. An image is worth 16x16 words: Transformers for image recognition at scale. In *9th International Conference on Learning Representations, ICLR 2021, Virtual Event, Austria, May 3-7, 2021*. OpenReview.net, 2021. [4](#)
- [11] Deng-Ping Fan, Cheng Gong, Yang Cao, Bo Ren, Ming-Ming Cheng, and Ali Borji. Enhanced-alignment measure for binary foreground map evaluation. In *Proceedings of the Twenty-Seventh International Joint Conference on Artificial Intelligence, IJCAI 2018, July 13-19, 2018, Stockholm, Sweden*, pages 698–704. ijcai.org, 2018. [7](#)
- [12] Deng-Ping Fan, Wenguan Wang, Ming-Ming Cheng, and Jianbing Shen. Shifting more attention to video salient object detection. In *IEEE Conference on Computer Vision and Pattern Recognition, CVPR 2019, Long Beach, CA, USA, June 16-20, 2019*, pages 8554–8564. Computer Vision Foundation / IEEE, 2019. [1](#)
- [13] Deng-Ping Fan, Zheng Lin, Zhao Zhang, Menglong Zhu, and Ming-Ming Cheng. Rethinking RGB-D salient object detection: Models, data sets, and large-scale benchmarks. *IEEE Trans. Neural Networks Learn. Syst.*, 32(5):2075–2089, 2021. [6](#)
- [14] Mengyang Feng, Huchuan Lu, and Errui Ding. Attentive feedback network for boundary-aware salient object detection. In *IEEE Conference on Computer Vision and Pattern Recognition, CVPR 2019, Long Beach, CA, USA, June 16-20, 2019*, pages 1623–1632. Computer Vision Foundation / IEEE, 2019. [6](#), [7](#)
- [15] Keren Fu, Deng-Ping Fan, Ge-Peng Ji, and Qijun Zhao. JL-DCF: joint learning and densely-cooperative fusion framework for RGB-D salient object detection. In *2020 IEEE/CVF Conference on Computer Vision and Pattern Recognition, CVPR 2020, Seattle, WA, USA, June 13-19, 2020*, pages 3049–3059. Computer Vision Foundation / IEEE, 2020. [1](#), [2](#)
- [16] Shanghua Gao, Ming-Ming Cheng, Kai Zhao, Xin-Yu Zhang, Ming-Hsuan Yang, and Philip H. S. Torr. Res2net: A new multi-scale backbone architecture. *IEEE Trans. Pattern Anal. Mach. Intell.*, 43(2):652–662, 2021. [2](#)
- [17] Chongjian Ge, Junsong Chen, Enze Xie, Zhongdao Wang, Lanqing Hong, Huchuan Lu, Zhenguo Li, and Ping Luo. Metabev: Solving sensor failures for 3d detection and map segmentation. In *Proceedings of the IEEE/CVF International Conference on Computer Vision (ICCV)*, pages 8721–8731, 2023. [1](#), [2](#)
- [18] Anjith George, Zohreh Mostaani, David Geissenbuhler, Olegs Nikisins, André Anjos, and Sébastien Marcel. Biometric face presentation attack detection with multi-channel convolutional neural network. *IEEE Trans. Inf. Forensics Secur.*, 15:42–55, 2020. [1](#)
- [19] Clément Godard, Oisín Mac Aodha, and Gabriel J. Brostow. Unsupervised monocular depth estimation with left-right consistency. In *2017 IEEE Conference on Computer Vision and Pattern Recognition, CVPR 2017, Honolulu, HI, USA, July 21-26, 2017*, pages 6602–6611. IEEE Computer Society, 2017. [4](#)
- [20] Kaiming He, Xiangyu Zhang, Shaoqing Ren, and Jian Sun. Deep residual learning for image recognition. In *2016 IEEE*

- Conference on Computer Vision and Pattern Recognition, CVPR 2016, Las Vegas, NV, USA, June 27-30, 2016*, pages 770–778. IEEE Computer Society, 2016. [2](#), [14](#)
- [21] Wei Ji, Jingjing Li, Shuang Yu, Miao Zhang, Yongri Piao, Shunyu Yao, Qi Bi, Kai Ma, Yefeng Zheng, Huchuan Lu, and Li Cheng. Calibrated RGB-D salient object detection. In *IEEE Conference on Computer Vision and Pattern Recognition, CVPR 2021, virtual, June 19-25, 2021*, pages 9471–9481. Computer Vision Foundation / IEEE, 2021. [2](#), [6](#), [7](#)
- [22] Wei Ji, Jingjing Li, Qi Bi, Chuan Guo, Jie Liu, and Li Cheng. Promoting saliency from depth: Deep unsupervised RGB-D saliency detection. In *The Tenth International Conference on Learning Representations, ICLR 2022, Virtual Event, April 25-29, 2022*. OpenReview.net, 2022. [2](#)
- [23] Wei Ji, Ge Yan, Jingjing Li, Yongri Piao, Shunyu Yao, Miao Zhang, Li Cheng, and Huchuan Lu. DMRA: depth-induced multi-scale recurrent attention network for RGB-D saliency detection. *IEEE Trans. Image Process.*, 31:2321–2336, 2022. [1](#), [6](#)
- [24] Menglin Jia, Luming Tang, Bor-Chun Chen, Claire Cardie, Serge J. Belongie, Bharath Hariharan, and Ser-Nam Lim. Visual prompt tuning. In *Computer Vision - ECCV 2022 - 17th European Conference, Tel Aviv, Israel, October 23-27, 2022, Proceedings, Part XXXIII*, pages 709–727. Springer, 2022. [2](#), [3](#), [5](#)
- [25] Xiao Jin, Kang Yi, and Jing Xu. Moadnet: Mobile asymmetric dual-stream networks for real-time and lightweight RGB-D salient object detection. *IEEE Trans. Circuits Syst. Video Technol.*, 32(11):7632–7645, 2022. [6](#), [7](#)
- [26] Ran Ju, Ling Ge, Wenjing Geng, Tongwei Ren, and Gangshan Wu. Depth saliency based on anisotropic center-surround difference. In *2014 IEEE International Conference on Image Processing, ICIP 2014, Paris, France, October 27-30, 2014*, pages 1115–1119. IEEE, 2014. [6](#)
- [27] Aishik Konwer, Xiaoling Hu, Joseph Bae, Xuan Xu, Chao Chen, and Prateek Prasanna. Enhancing modality-agnostic representations via meta-learning for brain tumor segmentation. In *Proceedings of the IEEE/CVF International Conference on Computer Vision (ICCV)*, pages 21415–21425, 2023. [1](#), [2](#)
- [28] Alex Krizhevsky, Ilya Sutskever, and Geoffrey E. Hinton. Imagenet classification with deep convolutional neural networks. *Commun. ACM*, 60(6):84–90, 2017. [7](#)
- [29] Yi-Lun Lee, Yi-Hsuan Tsai, Wei-Chen Chiu, and Chen-Yu Lee. Multimodal prompting with missing modalities for visual recognition. In *IEEE/CVF Conference on Computer Vision and Pattern Recognition, CVPR 2023, Vancouver, BC, Canada, June 17-24, 2023*, pages 14943–14952. IEEE, 2023. [1](#), [2](#), [3](#)
- [30] Brian Lester, Rami Al-Rfou, and Noah Constant. The power of scale for parameter-efficient prompt tuning. In *Proceedings of the 2021 Conference on Empirical Methods in Natural Language Processing, EMNLP 2021, Virtual Event / Punta Cana, Dominican Republic, 7-11 November, 2021*, pages 3045–3059. Association for Computational Linguistics, 2021. [2](#)
- [31] Aixuan Li, Jing Zhang, Yunqiu Lv, Bowen Liu, Tong Zhang, and Yuchao Dai. Uncertainty-aware joint salient object and camouflaged object detection. In *IEEE Conference on Computer Vision and Pattern Recognition, CVPR 2021, virtual, June 19-25, 2021*, pages 10071–10081. Computer Vision Foundation / IEEE, 2021. [2](#)
- [32] Guanbin Li and Yizhou Yu. Visual saliency based on multiscale deep features. In *IEEE Conference on Computer Vision and Pattern Recognition, CVPR 2015, Boston, MA, USA, June 7-12, 2015*, pages 5455–5463. IEEE Computer Society, 2015. [6](#)
- [33] Ge Li and Chunbiao Zhu. A three-pathway psychobiological framework of salient object detection using stereoscopic technology. In *2017 IEEE International Conference on Computer Vision Workshops, ICCV Workshops 2017, Venice, Italy, October 22-29, 2017*, pages 3008–3014. IEEE Computer Society, 2017. [6](#)
- [34] Gongyang Li, Zhi Liu, Minyu Chen, Zhen Bai, Weisi Lin, and Haibin Ling. Hierarchical alternate interaction network for RGB-D salient object detection. *IEEE Trans. Image Process.*, 30:3528–3542, 2021. [6](#), [7](#)
- [35] Hao Li, Dingwen Zhang, Nian Liu, Lechao Cheng, Yalun Dai, Chao Zhang, Xinggang Wang, and Junwei Han. Boosting low-data instance segmentation by unsupervised pre-training with saliency prompt. In *IEEE/CVF Conference on Computer Vision and Pattern Recognition, CVPR 2023, Vancouver, BC, Canada, June 17-24, 2023*, pages 15485–15494. IEEE, 2023. [1](#)
- [36] Yin Li, Xiaodi Hou, Christof Koch, James M. Rehg, and Alan L. Yuille. The secrets of salient object segmentation. In *2014 IEEE Conference on Computer Vision and Pattern Recognition, CVPR 2014, Columbus, OH, USA, June 23-28, 2014*, pages 280–287. IEEE Computer Society, 2014. [6](#)
- [37] Jiang-Jiang Liu, Qibin Hou, Ming-Ming Cheng, Jiashi Feng, and Jianmin Jiang. A simple pooling-based design for real-time salient object detection. In *IEEE Conference on Computer Vision and Pattern Recognition, CVPR 2019, Long Beach, CA, USA, June 16-20, 2019*, pages 3917–3926. Computer Vision Foundation / IEEE, 2019. [6](#), [7](#)
- [38] Jiang-Jiang Liu, Qibin Hou, Zhi-Ang Liu, and Ming-Ming Cheng. Poolnet+: Exploring the potential of pooling for salient object detection. *IEEE Trans. Pattern Anal. Mach. Intell.*, 45(1):887–904, 2023. [2](#)
- [39] Nian Liu, Junwei Han, and Ming-Hsuan Yang. Picanet: Pixel-wise contextual attention learning for accurate saliency detection. *IEEE Trans. Image Process.*, 29:6438–6451, 2020. [2](#)
- [40] Nian Liu, Ni Zhang, and Junwei Han. Learning selective self-mutual attention for RGB-D saliency detection. In *2020 IEEE/CVF Conference on Computer Vision and Pattern Recognition, CVPR 2020, Seattle, WA, USA, June 13-19, 2020*, pages 13753–13762. Computer Vision Foundation / IEEE, 2020. [1](#)
- [41] Nian Liu, Ni Zhang, Kaiyuan Wan, Ling Shao, and Junwei Han. Visual saliency transformer. In *2021 IEEE/CVF International Conference on Computer Vision, ICCV 2021*,

- Montreal, QC, Canada, October 10-17, 2021, pages 4702–4712. IEEE, 2021. [1](#), [2](#), [6](#), [7](#)
- [42] Pengfei Liu, Weizhe Yuan, Jinlan Fu, Zhengbao Jiang, Hiroaki Hayashi, and Graham Neubig. Pre-train, prompt, and predict: A systematic survey of prompting methods in natural language processing. *ACM Comput. Surv.*, 55(9):195:1–195:35, 2023. [2](#)
- [43] Ze Liu, Yutong Lin, Yue Cao, Han Hu, Yixuan Wei, Zheng Zhang, Stephen Lin, and Baining Guo. Swin transformer: Hierarchical vision transformer using shifted windows. In *2021 IEEE/CVF International Conference on Computer Vision, ICCV 2021, Montreal, QC, Canada, October 10-17, 2021*, pages 9992–10002. IEEE, 2021. [4](#), [7](#), [14](#)
- [44] Zhengyi Liu, Yacheng Tan, Qian He, and Yun Xiao. Swin-net: Swin transformer drives edge-aware RGB-D and RGB-T salient object detection. *IEEE Trans. Circuits Syst. Video Technol.*, 32(7):4486–4497, 2022. [1](#), [2](#), [4](#), [7](#), [15](#)
- [45] Ilya Loshchilov and Frank Hutter. Decoupled weight decay regularization. In *7th International Conference on Learning Representations, ICLR 2019, New Orleans, LA, USA, May 6-9, 2019*. OpenReview.net, 2019. [7](#)
- [46] Mingcan Ma, Changqun Xia, and Jia Li. Pyramidal feature shrinking for salient object detection. In *Thirty-Fifth AAAI Conference on Artificial Intelligence, AAAI 2021, Thirty-Third Conference on Innovative Applications of Artificial Intelligence, IAAI 2021, The Eleventh Symposium on Educational Advances in Artificial Intelligence, EAAI 2021, Virtual Event, February 2-9, 2021*, pages 2311–2318. AAAI Press, 2021. [6](#), [7](#)
- [47] Mingcan Ma, Changqun Xia, Chenxi Xie, Xiaowu Chen, and Jia Li. Boosting broader receptive fields for salient object detection. *IEEE Trans. Image Process.*, 32:1026–1038, 2023. [1](#), [2](#), [6](#), [7](#), [14](#), [15](#)
- [48] Shuai Ma, Kechen Song, Hongwen Dong, Hongkun Tian, and Yunhui Yan. Modal complementary fusion network for RGB-T salient object detection. *Appl. Intell.*, 53(8):9038–9055, 2023. [7](#)
- [49] Ran Margolin, Lih Zelnik-Manor, and Ayellet Tal. How to evaluate foreground maps. In *2014 IEEE Conference on Computer Vision and Pattern Recognition, CVPR 2014, Columbus, OH, USA, June 23-28, 2014*, pages 248–255. IEEE Computer Society, 2014. [7](#)
- [50] Fausto Milletari, Nassir Navab, and Seyed-Ahmad Ahmadi. V-net: Fully convolutional neural networks for volumetric medical image segmentation. In *Fourth International Conference on 3D Vision, 3DV 2016, Stanford, CA, USA, October 25-28, 2016*, pages 565–571. IEEE Computer Society, 2016. [4](#)
- [51] Vida Movahedi and James H. Elder. Design and perceptual validation of performance measures for salient object segmentation. In *IEEE Conference on Computer Vision and Pattern Recognition, CVPR Workshops 2010, San Francisco, CA, USA, 13-18 June, 2010*, pages 49–56. IEEE Computer Society, 2010. [6](#)
- [52] Tran Xuan Bach Nguyen, Kent Rosser, and Javaan S. Chahl. A review of modern thermal imaging sensor technology and applications for autonomous aerial navigation. *J. Imaging*, 7(10):217, 2021. [1](#)
- [53] Yuzhen Niu, Yujie Geng, Xueqing Li, and Feng Liu. Leveraging stereopsis for saliency analysis. In *2012 IEEE Conference on Computer Vision and Pattern Recognition, Providence, RI, USA, June 16-21, 2012*, pages 454–461. IEEE Computer Society, 2012. [6](#)
- [54] Youwei Pang, Xiaoqi Zhao, Lihe Zhang, and Huchuan Lu. Multi-scale interactive network for salient object detection. In *2020 IEEE/CVF Conference on Computer Vision and Pattern Recognition, CVPR 2020, Seattle, WA, USA, June 13-19, 2020*, pages 9410–9419. Computer Vision Foundation / IEEE, 2020. [4](#), [6](#), [7](#)
- [55] Youwei Pang, Xiaoqi Zhao, Lihe Zhang, and Huchuan Lu. CAVER: cross-modal view-mixed transformer for bi-modal salient object detection. *IEEE Trans. Image Process.*, 32:892–904, 2023. [2](#), [4](#), [6](#), [7](#), [14](#), [15](#)
- [56] Houwen Peng, Bing Li, Weihua Xiong, Weiming Hu, and Rongrong Ji. RGBD salient object detection: A benchmark and algorithms. In *Computer Vision - ECCV 2014 - 13th European Conference, Zurich, Switzerland, September 6-12, 2014, Proceedings, Part III*, pages 92–109. Springer, 2014. [6](#)
- [57] Federico Perazzi, Philipp Krähenbühl, Yael Pritch, and Alexander Hornung. Saliency filters: Contrast based filtering for salient region detection. In *2012 IEEE Conference on Computer Vision and Pattern Recognition, Providence, RI, USA, June 16-21, 2012*, pages 733–740. IEEE Computer Society, 2012. [7](#)
- [58] Yongri Piao, Wei Ji, Jingjing Li, Miao Zhang, and Huchuan Lu. Depth-induced multi-scale recurrent attention network for saliency detection. In *2019 IEEE/CVF International Conference on Computer Vision, ICCV 2019, Seoul, Korea (South), October 27 - November 2, 2019*, pages 7253–7262. IEEE, 2019. [2](#)
- [59] Xuebin Qin, Zichen Zhang, Chenyang Huang, Chao Gao, Masood Dehghan, and Martin Jägersand. Basnet: Boundary-aware salient object detection. In *IEEE Conference on Computer Vision and Pattern Recognition, CVPR 2019, Long Beach, CA, USA, June 16-20, 2019*, pages 7479–7489. Computer Vision Foundation / IEEE, 2019. [2](#), [4](#), [6](#), [7](#)
- [60] Karen Simonyan and Andrew Zisserman. Very deep convolutional networks for large-scale image recognition. In *3rd International Conference on Learning Representations, ICLR 2015, San Diego, CA, USA, May 7-9, 2015, Conference Track Proceedings*, 2015. [2](#)
- [61] Fuming Sun, Peng Ren, Bowen Yin, Fasheng Wang, and Haojie Li. Catnet: A cascaded and aggregated transformer network for rgb-d salient object detection. *IEEE Transactions on Multimedia*, pages 1–14, 2023. [6](#), [7](#), [14](#), [15](#)
- [62] Peng Sun, Wenhui Zhang, Huanyu Wang, Songyuan Li, and Xi Li. Deep RGB-D saliency detection with depth-sensitive attention and automatic multi-modal fusion. In *IEEE Conference on Computer Vision and Pattern Recognition, CVPR 2021, virtual, June 19-25, 2021*, pages 1407–1417. Computer Vision Foundation / IEEE, 2021. [2](#), [6](#), [7](#)
- [63] Bin Tang, Zhengyi Liu, Yacheng Tan, and Qian He. Hrtransnet: Hrformer-driven two-modality salient object

- detection. *IEEE Trans. Circuits Syst. Video Technol.*, 33(2):728–742, 2023. 2, 6, 7
- [64] Jin Tang, Dongzhe Fan, Xiaoxiao Wang, Zhengzheng Tu, and Chenglong Li. RGBT salient object detection: Benchmark and A novel cooperative ranking approach. *IEEE Trans. Circuits Syst. Video Technol.*, 30(12):4421–4433, 2020. 6
- [65] Xinyu Tian, Jing Zhang, Mochu Xiang, and Yuchao Dai. Modeling the distributional uncertainty for salient object detection models. In *IEEE/CVF Conference on Computer Vision and Pattern Recognition, CVPR 2023, Vancouver, BC, Canada, June 17-24, 2023*, pages 19660–19670. IEEE, 2023. 1, 2
- [66] Cheng-Hao Tu, Zheda Mai, and Wei-Lun Chao. Visual query tuning: Towards effective usage of intermediate representations for parameter and memory efficient transfer learning. In *IEEE/CVF Conference on Computer Vision and Pattern Recognition, CVPR 2023, Vancouver, BC, Canada, June 17-24, 2023*, pages 7725–7735. IEEE, 2023. 3
- [67] Zhengzheng Tu, Yan Ma, Zhun Li, Chenglong Li, Jieming Xu, and Yongtao Liu. RGBT salient object detection: A large-scale dataset and benchmark. *CoRR*, abs/2007.03262, 2020. 1, 2, 6
- [68] Zhengzheng Tu, Tian Xia, Chenglong Li, Xiaoxiao Wang, Yan Ma, and Jin Tang. RGB-T image saliency detection via collaborative graph learning. *IEEE Trans. Multim.*, 22(1):160–173, 2020. 6
- [69] Zhengzheng Tu, Zhun Li, Chenglong Li, Yang Lang, and Jin Tang. Multi-interactive dual-decoder for rgb-thermal salient object detection. *IEEE Trans. Image Process.*, 30:5678–5691, 2021. 1, 2, 4
- [70] Zhengzheng Tu, Zhun Li, Chenglong Li, and Jin Tang. Weakly alignment-free RGBT salient object detection with deep correlation network. *IEEE Trans. Image Process.*, 31:3752–3764, 2022. 2, 6
- [71] Ashish Vaswani, Noam Shazeer, Niki Parmar, Jakob Uszkoreit, Llion Jones, Aidan N. Gomez, Lukasz Kaiser, and Illia Polosukhin. Attention is all you need. In *Advances in Neural Information Processing Systems 30: Annual Conference on Neural Information Processing Systems 2017, December 4-9, 2017, Long Beach, CA, USA*, pages 5998–6008, 2017. 2
- [72] Lijun Wang, Huchuan Lu, Yifan Wang, Mengyang Feng, Dong Wang, Baocai Yin, and Xiang Ruan. Learning to detect salient objects with image-level supervision. In *2017 IEEE Conference on Computer Vision and Pattern Recognition, CVPR 2017, Honolulu, HI, USA, July 21-26, 2017*, pages 3796–3805. IEEE Computer Society, 2017. 6
- [73] Wenguan Wang, Shuyang Zhao, Jianbing Shen, Steven C. H. Hoi, and Ali Borji. Salient object detection with pyramid attention and salient edges. In *IEEE Conference on Computer Vision and Pattern Recognition, CVPR 2019, Long Beach, CA, USA, June 16-20, 2019*, pages 1448–1457. Computer Vision Foundation / IEEE, 2019. 2
- [74] Wenguan Wang, Qiuxia Lai, Huazhu Fu, Jianbing Shen, Haibin Ling, and Ruigang Yang. Salient object detection in the deep learning era: An in-depth survey. *IEEE Trans. Pattern Anal. Mach. Intell.*, 44(6):3239–3259, 2022. 2
- [75] Yifan Wang, Wenbo Zhang, Lijun Wang, Ting Liu, and Huchuan Lu. Multi-source uncertainty mining for deep unsupervised saliency detection. In *IEEE/CVF Conference on Computer Vision and Pattern Recognition, CVPR 2022, New Orleans, LA, USA, June 18-24, 2022*, pages 11717–11726. IEEE, 2022. 2
- [76] Yi Wang, Ruili Wang, Xin Fan, Tianzhu Wang, and Xi-angjian He. Pixels, regions, and objects: Multiple enhancement for salient object detection. In *IEEE/CVF Conference on Computer Vision and Pattern Recognition, CVPR 2023, Vancouver, BC, Canada, June 17-24, 2023*, pages 10031–10040. IEEE, 2023. 2, 4, 6, 7
- [77] Jun Wei, Shuhui Wang, and Qingming Huang. F³net: Fusion, feedback and focus for salient object detection. In *The Thirty-Fourth AAAI Conference on Artificial Intelligence, AAAI 2020, The Thirty-Second Innovative Applications of Artificial Intelligence Conference, IAAI 2020, The Tenth AAAI Symposium on Educational Advances in Artificial Intelligence, EAAI 2020, New York, NY, USA, February 7-12, 2020*, pages 12321–12328. AAAI Press, 2020. 2, 6, 7
- [78] Jun Wei, Shuhui Wang, Zhe Wu, Chi Su, Qingming Huang, and Qi Tian. Label decoupling framework for salient object detection. In *2020 IEEE/CVF Conference on Computer Vision and Pattern Recognition, CVPR 2020, Seattle, WA, USA, June 13-19, 2020*, pages 13022–13031. Computer Vision Foundation / IEEE, 2020. 2, 6, 7
- [79] Yu-Huan Wu, Yun Liu, Jun Xu, Jia-Wang Bian, Yuchao Gu, and Ming-Ming Cheng. Mobilesal: Extremely efficient RGB-D salient object detection. *IEEE Trans. Pattern Anal. Mach. Intell.*, 44(12):10261–10269, 2022. 4, 6, 7
- [80] Yu-Huan Wu, Yun Liu, Le Zhang, Ming-Ming Cheng, and Bo Ren. EDN: salient object detection via extremely-downsampled network. *IEEE Trans. Image Process.*, 31:3125–3136, 2022. 2, 6, 7, 14, 15
- [81] Zhe Wu, Li Su, and Qingming Huang. Cascaded partial decoder for fast and accurate salient object detection. In *IEEE Conference on Computer Vision and Pattern Recognition, CVPR 2019, Long Beach, CA, USA, June 16-20, 2019*, pages 3907–3916. Computer Vision Foundation / IEEE, 2019. 2, 6, 7
- [82] Chenxi Xie, Changqun Xia, Mingcan Ma, Zhirui Zhao, Xiaowu Chen, and Jia Li. Pyramid grafting network for one-stage high resolution saliency detection. In *IEEE/CVF Conference on Computer Vision and Pattern Recognition, CVPR 2022, New Orleans, LA, USA, June 18-24, 2022*, pages 11707–11716. IEEE, 2022. 2
- [83] Binwei Xu, Haoran Liang, Ronghua Liang, and Peng Chen. Locate globally, segment locally: A progressive architecture with knowledge review network for salient object detection. In *Thirty-Fifth AAAI Conference on Artificial Intelligence, AAAI 2021, Thirty-Third Conference on Innovative Applications of Artificial Intelligence, IAAI 2021, The Eleventh Symposium on Educational Advances in Artificial Intelligence, EAAI 2021, Virtual Event, February 2-9, 2021*, pages 3004–3012. AAAI Press, 2021. 6, 7
- [84] Qiong Yan, Li Xu, Jianping Shi, and Jiaya Jia. Hierarchical saliency detection. In *2013 IEEE Conference on Computer Vision and Pattern Recognition, Portland, OR, USA, June*

- 23-28, 2013, pages 1155–1162. IEEE Computer Society, 2013. 6
- [85] Chuan Yang, Lihe Zhang, Huchuan Lu, Xiang Ruan, and Ming-Hsuan Yang. Saliency detection via graph-based manifold ranking. In *2013 IEEE Conference on Computer Vision and Pattern Recognition, Portland, OR, USA, June 23-28, 2013*, pages 3166–3173. IEEE Computer Society, 2013. 6
- [86] Yi Ke Yun and Weisi Lin. Towards a complete and detail-preserved salient object detection. *IEEE Transactions on Multimedia*, pages 1–15, 2023. 6, 7
- [87] Yi Ke Yun and Takahiro Tsubono. Recursive contour-saliency blending network for accurate salient object detection. In *IEEE/CVF Winter Conference on Applications of Computer Vision, WACV 2022, Waikoloa, HI, USA, January 3-8, 2022*, pages 1360–1370. IEEE, 2022. 2
- [88] Jing Zhang, Deng-Ping Fan, Yuchao Dai, Saeed Anwar, Fatemeh Sadat Saleh, Tong Zhang, and Nick Barnes. Ucnnet: Uncertainty inspired RGB-D saliency detection via conditional variational autoencoders. In *2020 IEEE/CVF Conference on Computer Vision and Pattern Recognition, CVPR 2020, Seattle, WA, USA, June 13-19, 2020*, pages 8579–8588. Computer Vision Foundation / IEEE, 2020. 1, 2
- [89] Pingping Zhang, Wei Liu, Dong Wang, Yinjie Lei, Hongyu Wang, and Huchuan Lu. Non-rigid object tracking via deep multi-scale spatial-temporal discriminative saliency maps. *Pattern Recognit.*, 100:107130, 2020. 1
- [90] Yuan-fang Zhang, Jiangbin Zheng, Wenjing Jia, Wenfeng Huang, Long Li, Nian Liu, Fei Li, and Xiangjian He. Deep RGB-D saliency detection without depth. *IEEE Trans. Multimed.*, 24:755–767, 2022. 2
- [91] Jiaying Zhao, Yang Cao, Deng-Ping Fan, Ming-Ming Cheng, Xuan-Yi Li, and Le Zhang. Contrast prior and fluid pyramid integration for RGBD salient object detection. In *IEEE Conference on Computer Vision and Pattern Recognition, CVPR 2019, Long Beach, CA, USA, June 16-20, 2019*, pages 3927–3936. Computer Vision Foundation / IEEE, 2019. 1
- [92] Jiaying Zhao, Jiang-Jiang Liu, Deng-Ping Fan, Yang Cao, Jufeng Yang, and Ming-Ming Cheng. Egnnet: Edge guidance network for salient object detection. In *2019 IEEE/CVF International Conference on Computer Vision, ICCV 2019, Seoul, Korea (South), October 27 - November 2, 2019*, pages 8778–8787. IEEE, 2019. 2
- [93] Xiaoqi Zhao, Youwei Pang, Lihe Zhang, Huchuan Lu, and Lei Zhang. Suppress and balance: A simple gated network for salient object detection. In *Computer Vision - ECCV 2020 - 16th European Conference, Glasgow, UK, August 23-28, 2020, Proceedings, Part II*, pages 35–51. Springer, 2020. 2, 6, 7
- [94] Xiaoqi Zhao, Youwei Pang, Lihe Zhang, and Huchuan Lu. Joint learning of salient object detection, depth estimation and contour extraction. *IEEE Trans. Image Process.*, 31: 7350–7362, 2022. 1, 2
- [95] Xiaoqi Zhao, Youwei Pang, Lihe Zhang, Huchuan Lu, and Xiang Ruan. Self-supervised pretraining for RGB-D salient object detection. In *Thirty-Sixth AAAI Conference on Artificial Intelligence, AAAI 2022, Thirty-Fourth Conference on Innovative Applications of Artificial Intelligence, IAAI 2022, The Twelfth Symposium on Educational Advances in Artificial Intelligence, EAAI 2022 Virtual Event, February 22 - March 1, 2022*, pages 3463–3471. AAAI Press, 2022. 6, 7
- [96] Huajun Zhou, Bo Qiao, Lingxiao Yang, Jianhuang Lai, and Xiaohua Xie. Texture-guided saliency distilling for unsupervised salient object detection. In *IEEE/CVF Conference on Computer Vision and Pattern Recognition, CVPR 2023, Vancouver, BC, Canada, June 17-24, 2023*, pages 7257–7267. IEEE, 2023. 1, 2, 6
- [97] Tao Zhou, Huazhu Fu, Geng Chen, Yi Zhou, Deng-Ping Fan, and Ling Shao. Specificity-preserving RGB-D saliency detection. In *2021 IEEE/CVF International Conference on Computer Vision, ICCV 2021, Montreal, QC, Canada, October 10-17, 2021*, pages 4661–4671. IEEE, 2021. 4, 6, 7
- [98] Wujie Zhou, Fan Sun, Qiuping Jiang, Runmin Cong, and Jenq-Neng Hwang. Wavenet: Wavelet network with knowledge distillation for RGB-T salient object detection. *IEEE Trans. Image Process.*, 32:3027–3039, 2023. 7
- [99] Wujie Zhou, Yun Zhu, Jingsheng Lei, Rongwang Yang, and Lu Yu. Lsnet: Lightweight spatial boosting network for detecting salient objects in rgb-thermal images. *IEEE Trans. Image Process.*, 32:1329–1340, 2023. 2, 6, 7, 15
- [100] Ziqi Zhou, Zheng Wang, Huchuan Lu, Song Wang, and Meijun Sun. Multi-type self-attention guided degraded saliency detection. In *The Thirty-Fourth AAAI Conference on Artificial Intelligence, AAAI 2020, The Thirty-Second Innovative Applications of Artificial Intelligence Conference, IAAI 2020, The Tenth AAAI Symposium on Educational Advances in Artificial Intelligence, EAAI 2020, New York, NY, USA, February 7-12, 2020*, pages 13082–13089. AAAI Press, 2020. 2
- [101] Jiawen Zhu, Simiao Lai, Xin Chen, Dong Wang, and Huchuan Lu. Visual prompt multi-modal tracking. In *IEEE/CVF Conference on Computer Vision and Pattern Recognition, CVPR 2023, Vancouver, BC, Canada, June 17-24, 2023*, pages 9516–9526. IEEE, 2023. 2, 3, 5
- [102] Mingchen Zhuge, Deng-Ping Fan, Nian Liu, Dingwen Zhang, Dong Xu, and Ling Shao. Salient object detection via integrity learning. *IEEE Trans. Pattern Anal. Mach. Intell.*, 45(3):3738–3752, 2023. 2, 6, 7, 14, 15

6. Supplementary Material

In this section, we provide ablation experiments for both the backbone and the proposed baseline SOD model in Table 5, and show the comparison between our UniSOD and advanced multi-modal models on single-modal datasets in Table 6. Fig. 8 and Fig. 9 show more visualizations for the proposed SPG block, and the effect of the number of transformer layers, respectively. Additionally, Fig. 10 illustrates the limitations of our method as well as future plans.

6.1. More Ablation Studies

To verify the impact of the backbone on our UniSOD, we also use ResNet50 [20] as the backbone, and the results are shown in the third and fourth rows of Table 5. Compared to the counterparts (i.e., the first and second rows) using the SwinB [43] backbone, the performance decreases overall due to the fact that the more powerful backbone (i.e., SwinB) is able to extract richer features for saliency cue mining. Nonetheless, the UniSOD_R is still overall superior compared to the models (i.e., CAVER [55] and EDN [80]) that also use the ResNet50 [20] backbone. In addition, UniSOD_R and Pre-trained model_R have more learnable parameters, which mainly comes from the larger channel dimension of features extracted by ResNet50 [20].

We also replace the proposed baseline SOD model with an existing advanced single-modal SOD model (i.e., ICON [102]), which also uses SwinB [43] as the backbone. The results are demonstrated in the fifth and sixth rows of Table 5, in which 'UniSOD_ICON' indicates that the ICON was used as a frozen pre-trained model driven by the modality-aware prompts to address both single-modal and multi-modal SOD tasks. By comparison, UniSOD_ICON exhibits a weaker performance than UniSOD, which indicates the effectiveness of the proposed baseline SOD model. In addition, UniSOD_ICON is also comparable to the advanced methods (i.e., CATNet [61] and BBRF [47]) that also use the SwinB backbone. On the other hand, compared with the original ICON [102], UniSOD_ICON achieves average improvements of the five datasets on the four evaluation metrics (E_ξ , S_α , F_β^ω , and MAE) by 1.5%, 1.2%, 1.7%, and 20.7%, respectively, which demonstrates that the proposed SPG block is capable of generating effective modality-aware prompts for fine-tuning regardless of the pre-trained model.

6.2. Comparison on Single-modal Datasets

In Table 6, we verify the performance of four recent advanced multi-modal SOD methods on two representative single-modal SOD datasets. Specifically, based on their released codes and parameter settings, we only replace the multi-modal inputs with two identical RGB modal inputs, and train on the single-modal SOD training set to

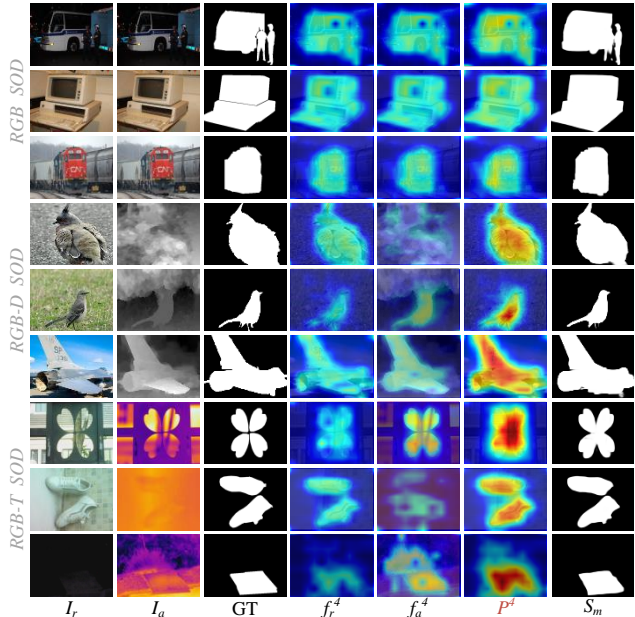


Figure 8. Feature visualization for the SPG block of the highest layer. I_r and I_a are input images, f_r^A and f_a^A are input features for SPG, P^A is the output prompt of SPG, S_m is the prediction, and GT is ground truth.

obtain corresponding models. It can be found that our UniSOD achieves a superior performance overall. This is mainly because our method is able to adequately learn the prior knowledge of the pre-trained SOD model through prompt tuning. Compared with the sub-optimal method CATNet [61], our method improves 1.6%, 0.8%, 4.1%, and 33.0% on the four metrics (E_ξ , S_α , F_β^ω , and MAE) of the two datasets, respectively. This is due to the fact that multi-modal models are only designed for multi-modal inputs to explore their complementary benefits, while our method can switch the structure based on single-modal and multi-modal inputs to generate modality-aware prompts for the pre-trained model.

6.3. More Feature Visualization

In Fig. 8, we show the feature visualization before and after the SPG block for more scenarios. For RGB SOD, the SPG block can refine and enhance single-modal input features for the prompts under low illumination (i.e., first row), large object (i.e., second row), and complex background (i.e., third row) challenges. For multi-modal SOD, the SPG block can exploit multi-modal complementary benefits to generate more robust features for the prompts in complex scenarios, such as auxiliary modality failure (i.e., fourth and eighth rows) or RGB modality being disturbed (i.e., fifth, seventh, and ninth rows).

Table 5. Ablation studies of the backbone and the proposed baseline SOD model on five representative single-modal and multi-modal datasets, with performance comparison to state-of-the-art methods. ‘-’ means that the method is not able to handle this dataset. The best results are marked with **bold**.

Model	Backbone	Params	DUTS				ECSSD				STERE				NJUD				VT5000			
			$E_{\xi} \uparrow$	$S_m \uparrow$	$F_{\beta}^{\omega} \uparrow$	$MAE \downarrow$	$E_{\xi} \uparrow$	$S_m \uparrow$	$F_{\beta}^{\omega} \uparrow$	$MAE \downarrow$	$E_{\xi} \uparrow$	$S_m \uparrow$	$F_{\beta}^{\omega} \uparrow$	$MAE \downarrow$	$E_{\xi} \uparrow$	$S_m \uparrow$	$F_{\beta}^{\omega} \uparrow$	$MAE \downarrow$	$E_{\xi} \uparrow$	$S_m \uparrow$	$F_{\beta}^{\omega} \uparrow$	$MAE \downarrow$
UniSOD Pre-trained model	SwinB	25.1	0.937	0.924	0.905	0.021	0.940	0.949	0.952	0.018	0.938	0.924	0.909	0.027	0.940	0.932	0.925	0.025	0.953	0.919	0.889	0.021
	SwinB	144.6	0.937	0.923	0.904	0.021	0.939	0.948	0.951	0.019	0.905	0.903	0.879	0.038	0.909	0.913	0.900	0.034	0.944	0.902	0.868	0.026
UniSOD_R Pre-trained model_R	ResNet50	100.3	0.907	0.893	0.851	0.033	0.930	0.933	0.931	0.025	0.934	0.910	0.887	0.033	0.923	0.907	0.888	0.037	0.932	0.895	0.847	0.030
	ResNet50	295.7	0.906	0.891	0.850	0.035	0.928	0.932	0.930	0.027	0.895	0.892	0.861	0.045	0.892	0.885	0.857	0.047	0.897	0.860	0.791	0.045
UniSOD_ICON ICON ₂₃ [102]	SwinB	25.1	0.935	0.919	0.892	0.023	0.938	0.945	0.944	0.020	0.933	0.921	0.896	0.031	0.930	0.929	0.914	0.028	0.946	0.910	0.866	0.025
	SwinB	92.4	0.930	0.917	0.886	0.025	0.932	0.941	0.936	0.023	0.901	0.902	0.873	0.041	0.904	0.910	0.888	0.038	0.941	0.898	0.852	0.028
CATNet ₂₃ [61] CAVER ₂₃ [55]	SwinB	263.1	-	-	-	-	-	-	-	-	0.935	0.921	0.900	0.030	0.932	0.932	0.921	0.026	-	-	-	-
	ResNet50	55.8	-	-	-	-	-	-	-	-	0.922	0.920	0.903	0.032	0.931	0.914	0.887	0.034	0.924	0.892	0.835	0.032
BBRF ₂₃ [47] EDN ₂₂ [80]	SwinB	74.1	0.927	0.909	0.886	0.025	0.934	0.939	0.944	0.022	-	-	-	-	-	-	-	-	-	-	-	-
	ResNet50	42.8	0.908	0.892	0.845	0.035	0.929	0.927	0.918	0.032	-	-	-	-	-	-	-	-	-	-	-	-

Table 6. Quantitative comparison with four advanced multi-modal methods on two representative single-modal datasets. The best results are marked with **bold**.

Model	DUTS				ECSSD			
	$E_{\xi} \uparrow$	$S_m \uparrow$	$F_{\beta}^{\omega} \uparrow$	$MAE \downarrow$	$E_{\xi} \uparrow$	$S_m \uparrow$	$F_{\beta}^{\omega} \uparrow$	$MAE \downarrow$
UniSOD	0.937	0.924	0.905	0.021	0.940	0.949	0.952	0.018
CATNet ₂₃ [61]	0.912	0.912	0.852	0.029	0.935	0.947	0.934	0.023
CAVER ₂₃ [55]	0.906	0.888	0.837	0.034	0.925	0.925	0.916	0.032
LSNet ₂₃ [99]	0.856	0.823	0.706	0.066	0.907	0.892	0.844	0.055
SwinNet ₂₂ [44]	0.904	0.907	0.855	0.031	0.932	0.942	0.933	0.025

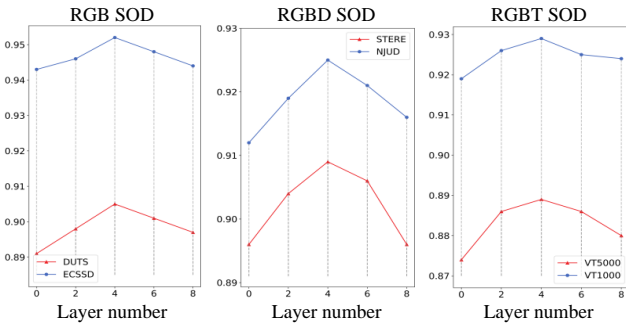


Figure 9. Effect of the number of transformer encoder layers on the proposed UniSOD.

6.4. Effect of Transformer Layers

Since the blended input with the appended modality-aware prompts mainly interacts in the transformer encoder, we verify the effect of the transformer encoder layers on our UniSOD. Fig. 9 illustrates the F_{β}^{ω} performance variation of UniSOD on both single-modal and multi-modal representative datasets. As the number of layers increases, the modality-aware prompts can interact with the inherent input more adequately to adapt the pre-trained model better to the corresponding task. However, when the number of layers exceeds 4, the performance shows a decreasing trend. This is mainly because more layers result in a larger number of parameters, but the limited training data makes it difficult to fit. Therefore, we adopt a 4-layer transformer encoder setting here.

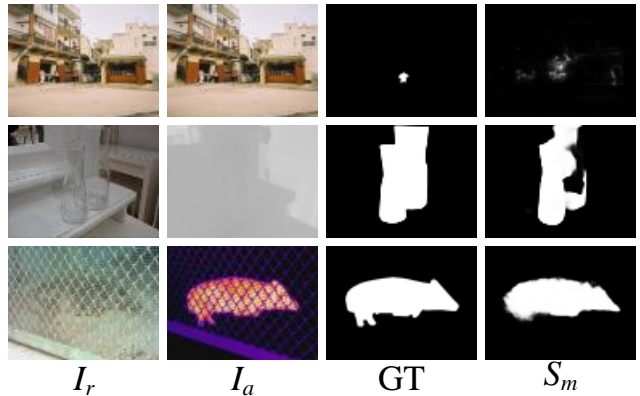


Figure 10. Visualization of some typical failure cases from RGB, RGB-D, and RGB-T test datasets.

6.5. Failure Cases and Future Works

Although our method achieves superior performance on both single-modal and multi-modal SOD tasks, it still fails in some extremely challenging scenarios, as shown in Fig 10. In the first row, the object of interest is difficult to be accurately localized due to the complex background and the tiny size of the object. The second row shows the difficulty of capturing complete transparent objects with low contrast and poor depth map. The third row demonstrates the difficulty of segmenting objects with clear boundaries under heavy occlusion. This is mainly due to the fact that these challenges are significantly difficult, and our UniSOD, which is a unified and general framework for multiple tasks, lacks a challenge-specific design.

To address this issue, we plan to add corresponding designs to the baseline SOD model in the future work, which can provide prior knowledge for downstream tasks to deal with these challenges. In addition, by optimizing the design of the SPG block for the characteristics of different tasks, prompts for specific challenges can be generated for the pre-trained model.